universität innsbruck

103rd AMS Annual Meeting, 8–12 January 2023
24th Symposium on Boundary Layers and Turbulence

Characteristics of a Cold Air Pool near Seefeld, Austria

Andreas Rauchöcker[1] (*andreas.rauchoecker@uibk.ac.at*), Manuela Lehner[1], Ivana Stiperski[1], and Alexander Rudolph[1,2]

[1]University of Innsbruck, Department of Atmospheric and Cryospheric Sciences, [2] Hessischer Rundfunk

SEECAP (Seefeld Cold-Air Pool Experiment)

SEECAP was a measurement campaign that took place in a valley close to Seefeld, Austria, between December 2019 and March 2020. This valley features two basins (upper UB and lower LB) separated by a minor ridge and is well-known for frequent occurrence of cold-air pools. The cold-air pool formation there is a small-scale phenomenon, as the valley is 3 km long, 300 m deep and the surrounding peaks are 2 km apart. The goal of SEECAP was to **identify the dominant processes** involved in cold-air pool formation and evolution in that valley.

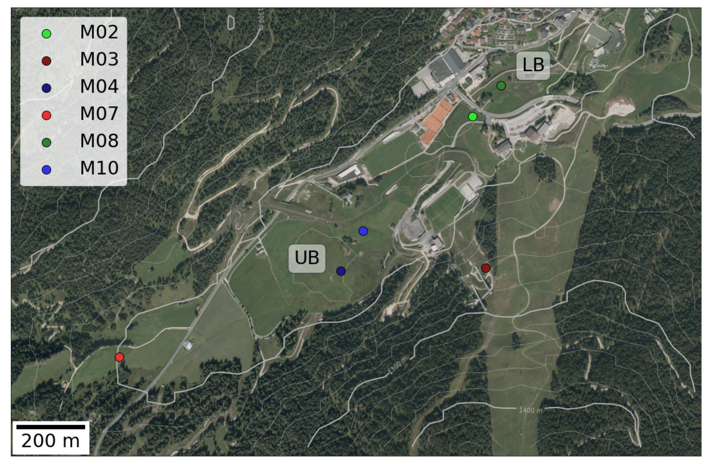

The measurement site including measurement stations.

Table: Six measurement stations and their characteristics in the field and in the model.

Site	True Elevation (m)	Characteristics	Distance reference grid point to station (m)	Elevation difference (m)
M02	1179	valley floor, LB	14 m	+1 m
M03	1260	cross-valley slope	12 m	+4 m
M04	1180	valley floor, UB	75 m	-1 m
M07	1200	along-valley slope	6 m	-3 m
M08	1179	valley floor, LB	19 m	+3 m
M10	1186	ridge, above UB	21 m	-4 m

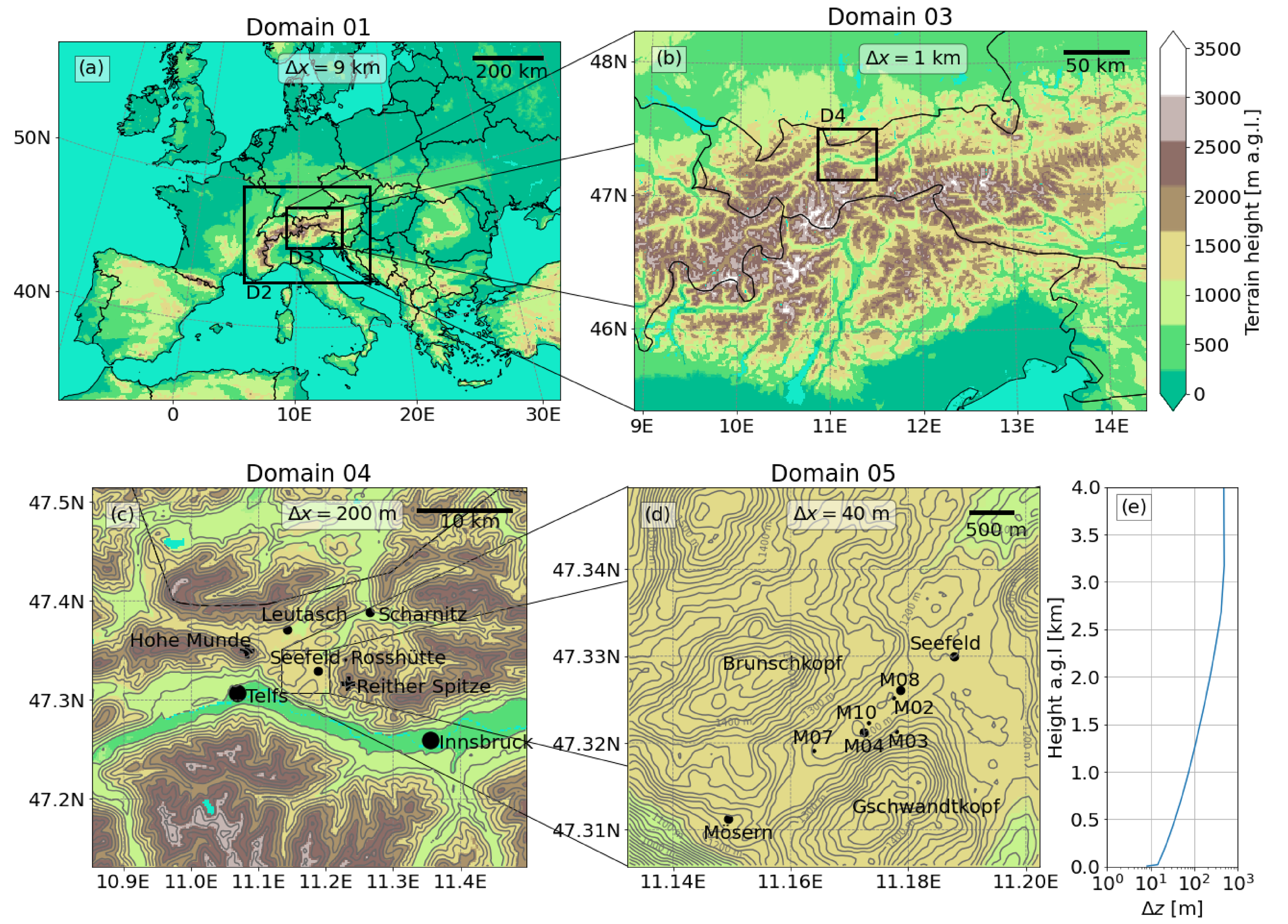

Model terrain and location of the measurement stations on the Seefeld Plateau, Austria.

High-resolution simulations with the Weather Research and Forecasting Model (WRF) were compared to measurements to identify the spatial characteristics of the cold-air pool. Results for the finest domain with $\Delta x = 40$ m are presented here. A case study featuring an **ideal cold-air pool evolution interrupted by a wind disturbance** was selected to exemplify formation and erosion processes. The night from January 16 to January 17 2020 was characterized by clear-sky conditions and a southwesterly flow above the mountains.

Comparison between measurement data and simulations

Temperature shows a typical cold-air pool formation: with an initial rapid temperature decrease, followed by reduced cooling rate. Around midnight, the cold-air pool was disturbed by increased wind speed related to foehn. Later, more quiescent conditions allowed the cold-air pool to reestablish. Three distinctly different **temperature and wind regimes** were observed:

- Higher temperature and wind speed at the stations above the basins (green) on the slopes suggested that the cold-air pool did not reach those stations.
- Lowest temperatures in UB (dark blue), but also strongest warming due to wind disturbance.
- Also low temperatures in LB (blue), but less affected by rising wind speed.

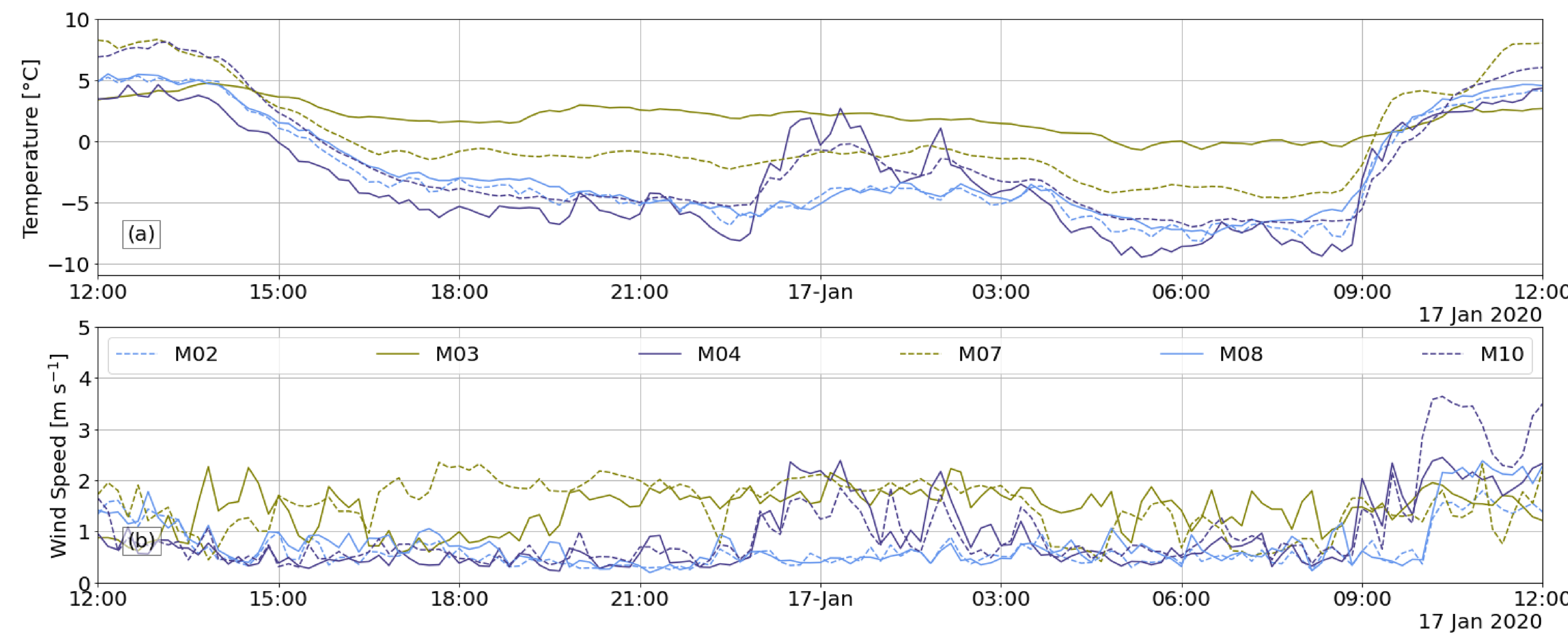

Measurement results at the six stations.

Although generally representing measurement results well, the **simulation results** at the reference grid points featured **higher wind speeds** within the basin, preventing

- an earlier cooling start after sunset,
- lower temperatures within UB before the disturbance,
- lower temperatures at the stations of LB during the disturbance, and
- a fully established cold-air pool after the erosion event.

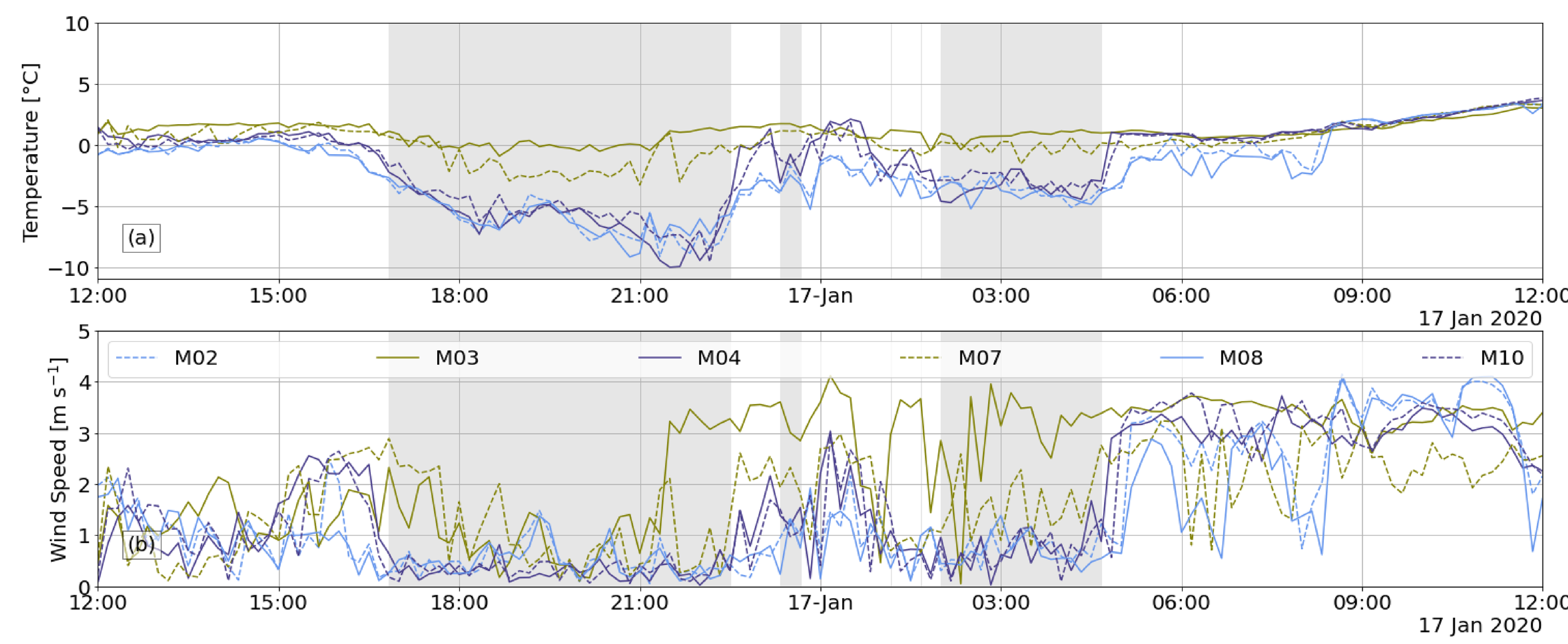

Simulation results at the reference grid point. Grey shading indicates temperature gradients of 4 K / 100 m or more at the reference grid point of M04.

Conclusion:

- The **simulation reproduced the measured temperature evolution** well: the established cold-air pool, its erosion by wind reformation of the cold-air pool.
- The primary sources of cooling within the valley were subgrid-scale, while advection and associated turbulent mixing eroded the cold-air pool.

Spatial structure during cooling periods

During periods with weak wind, a strong inversion developed in the basin with a strong **dependence of temperature on elevation**:

- Coldest temperatures occurred below 1190 m a.s.l.
- The strongest part of the inversion rarely extended to the second model level.

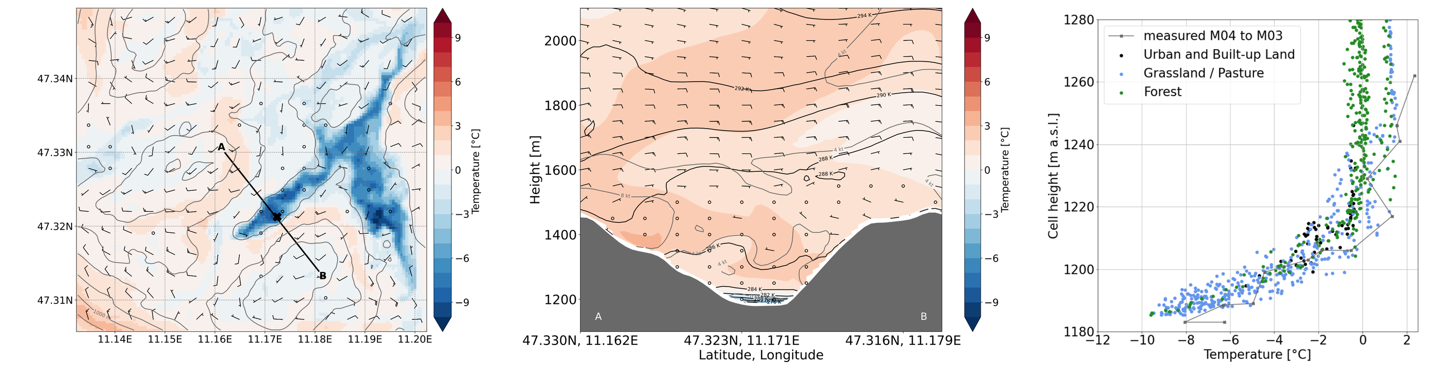

Temperature and wind at the lowest model level (left), for the cross section indicated (center) and temperature of all near-surface cells within the valley (right) at 2200 UTC January 16 2020.

Spatial structure during the erosion

Southwesterly flow, prevailing above crest height, penetrated temporarily into the basin.

- Short-lived rotors caused mixing and
- **Mixing and warm-air advection** eroded the cold-air pool.

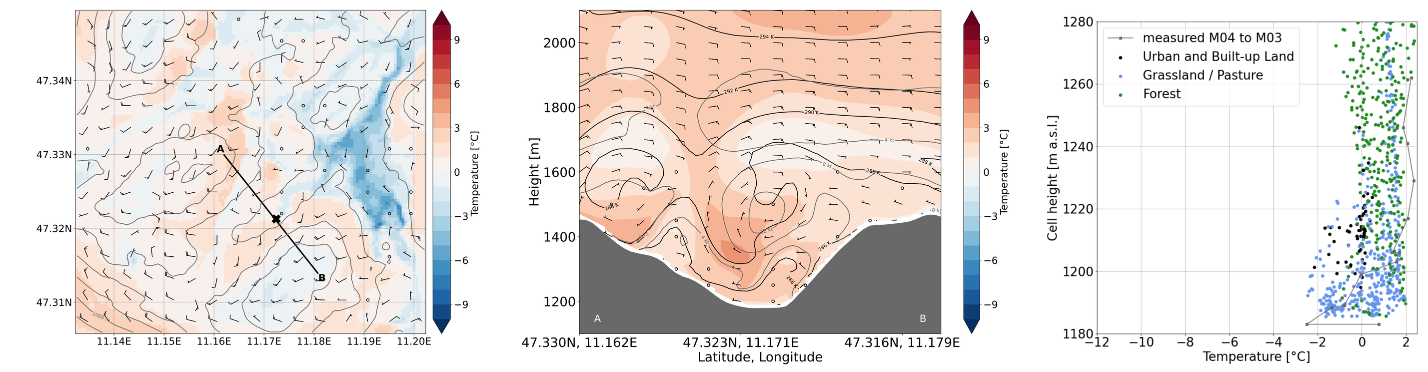

Temperature and wind at the lowest model level (left), for the cross section indicated (center) and temperature of all near-surface cells within the valley (right) at 0000 UTC January 17 2020.

Temperature tendency and cooling processes

- The **dominant cooling mechanisms** were **subgrid-scale turbulence and longwave radiation**
- Fog formation before midnight contributed to warming, when air was saturated.
- **Advection and resolved turbulence** had a net **warming contribution**.
- The combined warming effect of cross-valley flows and vertical advection during the first erosion event suggests that mixing due to downslope flows eroded the cold air.

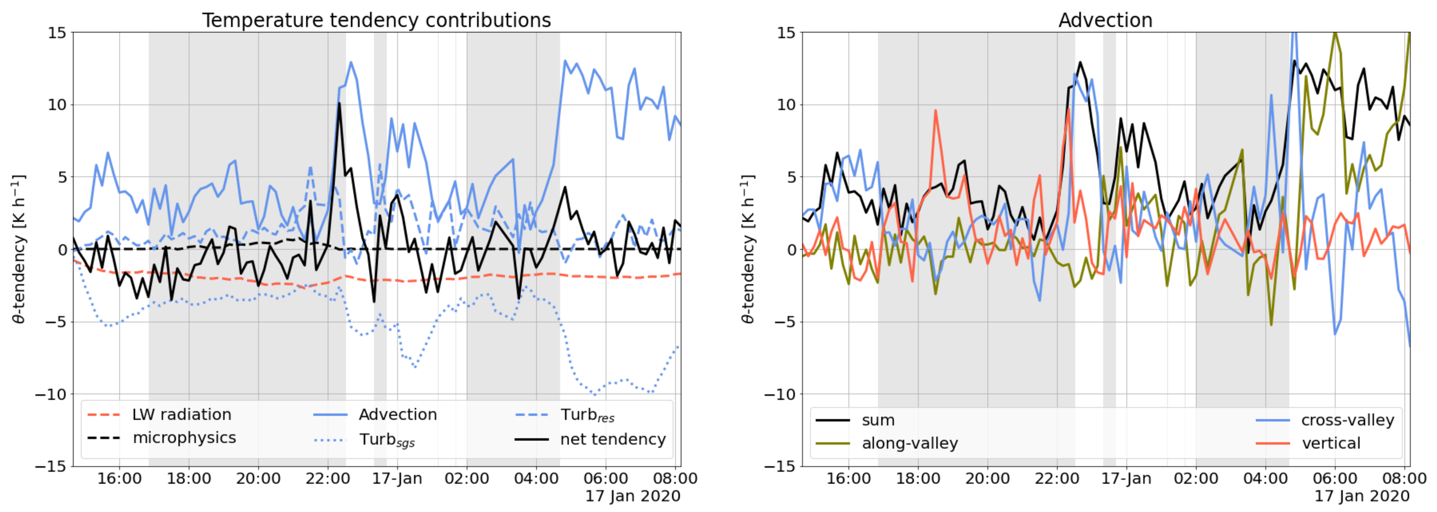

Temperature tendency from different cooling processes between 1440 UTC January 16 2020 and 0810 UTC January 17 2020 at the lowest model level averaged over all grid cells below 1190 m a.s.l. within the basin.

Acknowledgments: The computational results presented here have been achieved (in part) using the LEO HPC infrastructure of the University of Innsbruck and the Vienna Scientific Cluster (VSC). Funding: EGTC European Region Tyrol-South Tyrol-Trentino/Austrian Science Fund FWF - IPN 101-32